*Progress In Electromagnetics Research M, Vol. 36, 47–56, 2014*

# A Dual Grating Waveguide Structure for Wakefield Acceleration at THz

**Ganeswar Mishra and Geetanjali Sharma***

**Abstract**—A dual grating waveguide accelerator structure is investigated and compared with the dielectric wakefield accelerator at THz frequencies. In a dielectric wakefield accelerator, thinner liners for a given current and liners having lower dielectric constant are not preferable due to the fact that they generate much lower axial wakefields. This limits the operation of the device at THz. On the other hand, it is shown that a grating waveguide is tuned at THz with shallower slot heights with competitive wakefield gradients than a dielectric wakefield accelerator.

## 1. INTRODUCTION

As advanced accelerator concept, wakefield acceleration of charged particles in slow wave structure waveguides attracts much interest. In this scheme relativistic charged particle bunch excites electromagnetic wakefields in a slow wave structure waveguide. The wakefield is then used to accelerate a second trailing group of particle bunch to very high energies. There are two important wakefield accelerator concepts depending on the use of slow wave structure waveguide. A plasma wakefield accelerator [1–3] uses a plasma loaded waveguide. This is an electrostatic accelerator in which the accelerator mode is a large amplitude plasma wave. The dielectric wakefield accelerator [4–10] is the second one which uses a dielectric lined waveguide for wakefield acceleration. This is an electromagnetic accelerator that operates on the principle of Cerenkov radiation. Both the concepts have distinct advantages and disadvantages. The plasma supports large electric fields through ionization. This is the most attractive feature of the plasma wakefield accelerator. The second advantages of plasma wakefield accelerator is that it is a single mode device. This means that all the energy of the drive beam goes to the single mode giving rise to an efficient device. The disadvantage of plasma wakefield accelerator is its lower transform ratio in the high density regime of the plasma. On the other hand, the dielectric wakefield accelerator is a multimode device and requires suppression of higher order modes for the device to be as efficient as plasma wakefield accelerator. The effects of liner fluctuations are some other technical constraints of the dielectric wakefield accelerator. The advantage of the dielectric wakefield accelerator is that it operates at a much lower frequency than the plasma wakefield accelerator that is suitable for obtaining large transformer ratio through a desired pulse shaping. Ferrite loaded waveguide was also proposed for wakefield acceleration [11–13] as an alternative to dielectric wakefield acceleration. However, the ferrite loaded waveguide was more susceptible to dielectric breakdown and less popular in comparison to dielectric wakefield accelerator. It has been suggested to use metal grating waveguide as slow wave structure for beam wave interaction. When the grating waveguide is used as a slow wave structure, the radiation is Smith-Purcell Effect [14]. The effect has been effectively used to devise a laser known as Smith-Purcell free electron laser [15–19]. The grating guide is used in a variety of configurations. Improved performance from the grating waveguide has been extricated with sidewalls and dual grating structure [20–22]. The grating based FEL (i.e., Free Electron Laser) has

*Received 22 March 2014, Accepted 27 April 2014, Scheduled 5 May 2014*
* Corresponding author: Geetanjali Sharma (geetanjali.sharma678@gmail.com).
The authors are with the School of Physics, Devi Ahilya University, Indore, MP 452001, India.

been devised in two beams [23] with Bragg-gratings at the end [24] and in two-stage configuration [25]. In a grating waveguide, a mode exists, for which there is an electric field component in the direction of beam propagation, i.e., the relativistic beam interacts with the TM mode of the waveguide. The grating waveguide is a periodic structure, so the electric field is composed of space harmonics which have periodicity of the grating according to the Floquot's theorem. The axial electric field can be represented as,

$$E_z(x,z,t) = \sum_n E_{zn}(x) \exp\{i(k_n z - \omega t)\}, \quad k_n = k - 2n\pi/l$$

where $k_n$ is the wave number of the mode, $\omega$ the angular frequency of the mode, and $l$ the grating period. If one of the space harmonics has a phase velocity approximately the same as the electron velocity (i.e., $\omega = k_n v$), then the axial electric field can work on the electron beam, and stimulated emission occurs as the basis of the Smith-Purcell FEL.

In this paper, we propose dual grating waveguide for wakefield acceleration as an alternative application and compare the results with the conventional dielectric wakefield accelerator [26, 27]. The grating wakefield acceleration is very similar to dielectric wakefield accelerator, eliminates the disadvantage of dielectric breakdown, and can carry large amplitude beam current. In this device, the fundamental accelerating mode is the TM waveguide mode of the grating guide. The proposed grating wakefield accelerator is an electromagnetic accelerator that operates on the principle of Smith-Purcell radiation. In this paper, we derive the Fourier transformed wave equations using Maxwell's equations. The solutions of the wave equations are obtained in different regions of the dual grating-beam loaded waveguide. We use appropriate boundary conditions at the beam-vacuum-grating interface to derive the wakefield amplitude and frequency of the TM mode excited in the waveguide. The results are analyzed in compared with dielectric lined wakefield accelerator.

## 2. WAKEFIELD AMPLITUDE

The slow wave supporting structure of the proposed grating wakefield accelerator is a double-grating waveguide structure (Fig. 1). In Fig. 1, $d$ is the slot width, $h$ the slot height, and $l$ the grating period. It is assumed that the waveguide dimensions are infinite in the $y$-dimension. There is a beam-grating gap in the region $x_0 < x < a$. The electron beam has been chosen to be rectangular in shape with height $2x_0$. It is confined in the region $-x_0 < x < x_0$. Such a beam distribution in $x$ direction can be described by a current source of the form

$$\vec{j} = \hat{z}\rho_0 v\delta(z - vt)\{\Theta(|x_0| - x)\}$$

However, due to symmetric nature of the waveguide under consideration, appropriate boundary conditions are required on electric and displacement field vectors for either the upper or lower half of the waveguide to derive the dispersion relation of the waveguide. Hence it is appropriate to consider that the wakefield accelerator is driven by a charge and current density of the form,

$$\rho = \rho_0\delta(z - vt)\Theta(x_0 - x) \qquad \vec{j} = \hat{z}\rho_0 v\delta(z - vt)\Theta(x_0 - x) \tag{1}$$

The current propagates along $z$-axis of the dielectric wakefield accelerator with electron velocity $v$, beam half width $x_0$, and charge density $\rho_0$. In general, $x_0 \ll a$. From the linearized fluid and Maxwell

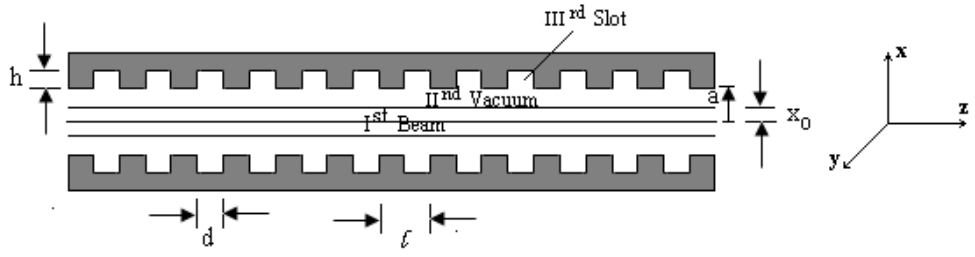


**Figure 1.** Schematic of grating wakefield accelerator.

equations, we write the wave equation for the $n$th axial field component of the TM mode

$$\frac{\partial^2 \vec{E}}{\partial x^2} + \frac{\partial^2 \vec{E}}{\partial z^2} - \frac{1}{c^2}\frac{\partial^2 \vec{E}}{\partial t^2} = 4\pi\nabla\rho - \frac{4\pi}{c^2}\frac{\partial \vec{j_b}}{\partial t} \tag{2}$$

Assume that the time dependency for the axial electric field $E_z$ is,

$$E_{zn}(x,z,t) = \frac{1}{2\pi v}\int\limits_{-\infty}^{+\infty} E_z(x,\omega)e^{i(\omega/v)(z-vt)}d\omega$$

And use

$$\delta(z-vt) = \frac{1}{2\pi v}\int\limits_{-\infty}^{+\infty} e^{i(\omega/v)(z-vt)}d\omega$$

We have following Fourier transformed wave equation,

$$\left[\frac{\partial^2}{\partial x^2} - \frac{\omega^2}{v^2}\left(1-\frac{v^2}{c^2}\right)\right]E_{zn}(x,\omega) = \frac{4\,\pi\,i\,v\rho_0}{\omega\gamma^2} \tag{3}$$

where $\gamma^2 = 1/1 - \left(v^2/c^2\right)$ is the relativistic factor and $v$ the velocity of the drive beam.

In the beam-grating vacuum gap, the wave equation is written as,

$$\left[\frac{\partial^2}{\partial x^2} - \frac{\omega^2}{\nu^2}\left(1-\frac{v^2}{c^2}\right)\right]E_{zn}(x,\omega) = 0$$

The solutions for the axial electric field in the different regions of the waveguide may be written as,

$$E^I_{zn}(x,\omega) = \frac{-4\pi i\rho_0}{\omega/\nu} + A\cosh\left(\frac{\omega x}{\nu\gamma}\right) \quad (x < x_0) \tag{4a}$$

$$E^{II}_{zn}(x,\omega) = B\cosh\left(\frac{\omega x}{\nu\gamma}\right) + C\sinh\left(\frac{\omega x}{\nu\gamma}\right) \quad (x_0 < x < a) \tag{4b}$$

In the slot region, the wave equation is solved by assuming that the field is standing wave solutions. Following Garate et al. [15], the solution reads,

$$E^{III}_{zn}(x,\omega) = \sum_m \sin\left[q_m\left\{x-(a+h)\right\}\right]\left\{D_m\cos\left(\frac{m\pi z}{d}\right) + E_m\sin\left(\frac{m\pi z}{d}\right)\right\} \tag{4c}$$

where

$$q_m^2 = \left\{\left(\omega^2/c^2\right) - \left(m\pi/d\right)^2\right\}$$

Eq. (4c) automatically satisfies the boundary condition that at $x = -(a+h)$, $E^{III}_z(x,\omega) = 0$

Assuming that the grating period is much less than the radiation wavelength, i.e., $l \ll \lambda$, then the axial electric field will not change much over the slot width. Hence the expression for the axial field can be approximated by $m = 0$ term.

$$E^{III}_{zn}(x,\omega) = D\sin\left[q\left\{x-(a+h)\right\}\right], \quad q^2 = \omega^2/c^2, \quad (d < z < l;\ a < x < a+h) \tag{4d}$$

Eq. (4a), Eq. (4b) and Eq. (4d) are the respective solutions in the beam region, beam-grating gap and in the slot. It is appropriate to mention here that we use a notation that $p^2 = \omega^2/v^2$, and subsequently in the limit $\nu \approx c$, we use $p^2 = k_n^2 = \omega^2/c^2$. Keeping this in mind, appropriate boundary conditions are used to derive the expression for the wakefield amplitude.

Using boundary conditions at the beam-vacuum interface, i.e., at, $x = x_0$, i.e., $E^I_{zn} = E^{II}_{zn}$ & $D^I_{xn} = D^{II}_{xn}$, we get,

$$\frac{-4\pi i\rho_0}{p} + A\cosh\left(\frac{px_0}{\gamma}\right) = B\cosh\left(\frac{px_0}{\gamma}\right) + C\sinh\left(\frac{px_0}{\gamma}\right) \tag{5a}$$

$$A\sinh\left(\frac{px_0}{\gamma}\right) = B\sinh\left(\frac{px_0}{\gamma}\right) + C\cosh\left(\frac{px_0}{\gamma}\right) \tag{5b}$$

Using boundary conditions at the vacuum-grating interface, i.e., $E_{zn}^{II}|_{x=a,\,along\,d} = E_{zn}^{III}$ & $\bar{B}_{yn}^{beam}|_{x=a,\,along\,d} = B_{yn}^{slotI}$, we get,

$$-D\sin\left(\frac{pvh}{c}\right)\left(\frac{d}{l}\right)\frac{\sin\left(k_n d/2\right)}{\left(k_n d/2\right)} = B\cosh\left(\frac{pa}{\gamma}\right) + C\sinh\left(\frac{pa}{\gamma}\right) \tag{6a}$$

$$D\cos\left(\frac{pvh}{c}\right) = \left(\frac{-pv}{c}\right)\left(\frac{\gamma}{p}\right)\frac{\sin\left(k_n d/2\right)}{\left(k_n d/2\right)}\left[B\sinh\left(\frac{pa}{\gamma}\right) + C\cosh\left(\frac{pa}{\gamma}\right)\right] \tag{6b}$$

Eqs. (6a) and (6b) can be used to get a relation between $B$ and $C$ as,

$$B = \Lambda_2 C \tag{7}$$

where

$$\Lambda_2 \;=\; \frac{\Lambda_1 \cos\,h\left(\frac{pa}{\gamma}\right) -\, \sin h\left(\frac{pa}{\gamma}\right)}{\cos\,h\left(\frac{pa}{\gamma}\right) -\, \Lambda_1 \sin h\left(\frac{pa}{\gamma}\right)} \tag{8}$$

$$\Lambda_1 \;=\; \left(\frac{pv}{c}\right)\left(\frac{\gamma}{p}\right)\left(\frac{d}{l}\right)\frac{\sin^2\left(k_n d/2\right)}{\left(k_n d/2\right)^2}\tan\left(\frac{\omega h}{c}\right) \tag{9}$$

Using Eq. (7), we rewrite Eqs. (5a) and (5b) as,

$$\frac{-4\pi i\rho_0}{p} + A\cosh\left(\frac{px_0}{\gamma}\right) \;=\; C\left[\Lambda_2\cosh\left(\frac{px_0}{\gamma}\right) + \sinh\left(\frac{px_0}{\gamma}\right)\right] \tag{10a}$$

$$A\sinh\left(\frac{px_0}{\gamma}\right) \;=\; C\left[\Lambda_2\sinh\left(\frac{px_0}{\gamma}\right) + \cosh\left(\frac{px_0}{\gamma}\right)\right] \tag{10b}$$

Eqs. (10a) and (10b) give the value of $A$ as,

$$A = \frac{4\pi i\rho_0}{p}\left[\Lambda_2\sinh\left(\frac{px_0}{\gamma}\right) + \cosh\left(\frac{px_0}{\gamma}\right)\right] \tag{11}$$

Eq. (11) helps to write the wakefield amplitude as,

$$\begin{aligned} E_z^I\left(x,p\right) \;=\; & \frac{-4\pi i\rho_0}{p}\left[1 - \cosh\left(\frac{px_0}{\gamma}\right)\cosh\left(\frac{px}{\gamma}\right)\right] \\ & + \frac{4\pi\, i\rho_0}{p}\cosh\left(\frac{px}{\gamma}\right)\sinh\left(\frac{px_0}{\gamma}\right)\left[\frac{\gamma b\cosh\left(\frac{pa}{\gamma}\right) - \sinh\left(\frac{pa}{\gamma}\right)}{\cosh\left(\frac{pa}{\gamma}\right) - \gamma b\sinh\left(\frac{pa}{\gamma}\right)}\right] \end{aligned} \tag{12a}$$

where

$$b = \frac{d}{l}\frac{v}{c}\frac{\sin^2\left(k_n d/2\right)}{\left(k_n d/2\right)^2}\tan\left(\frac{\omega h}{c}\right) \tag{12b}$$

Since most wakefield accelerators use drive beam with $v \approx c$, taking limit $v \to c$ Eq. (12) becomes,

$$E_z^I\left(x,p\right) = 4\pi i\rho_0 x_0\frac{d}{l}\left(\frac{\sin^2\left(k_n d/2\right)}{\left(k_n d/2\right)^2}\right)\left[\frac{\sin\left(ph\right)}{\cos\left(ph\right) - \left(d/l\right)pa\left(\frac{\sin^2\left(k_n d/2\right)}{\left(k_n d/2\right)^2}\right)\sin\left(ph\right)}\right] \tag{13}$$

The denominator in Eq. (13) is the dispersion relation of the grating waveguide, $p = k_n = \omega/c$ when $v \to c$. To rewrite time-dependent axial wakefield inverse Fourier transforming Eq. (13) and then

solving the integral as contour integral, we get time-dependant axial wakefield as

$$E_{zn}^{I}(x,z,t) = -4\pi\rho_0 x_0 \frac{d}{l}\sum_{n=0}^{\infty}\left[\frac{\sin(ph)\left(\frac{\sin^2(pd/2)}{(pd/2)^2}\right)}{D(a,d,h,p)}\right]\cos\left[p_m(z-ct)\right] \tag{14}$$

where

$$D(a,d,h,p) = -\left[hpa\frac{d}{l}\left(\frac{\sin^2(pd/2)}{(pd/2)^2}\right)\cos(ph) + \left\{a\frac{d}{l}\left(\frac{\sin^2(pd/2)}{(pd/2)^2}\right)+h\right\}\sin(ph)\right] \tag{15}$$

Writing the asymmetric current pulse distribution as,

$$\vec{j}(x,z-ct) = \hat{z}\rho_0 c\delta(x_0-x)\Theta(L-s)(s/L) \quad (s=z-ct)$$

Here '$L$' is pulse length, and $\rho_0 c$ defines the peak beam current density. Now using the convolution theorem,

$$E_z^I(x,y) = \int_0^{UL} dy' j(x,y') G(x,s-y')$$

Here, $G(x,s)$ defines the field generated for a delta function current distribution, $\delta(y)$, given by Eq. (14) in our case. The upper limit of integration, $UL = s$ if $s < L$, and $UL = L$ if $s > L$. We consider only the wakefield generated behind the beam ($s > L$). The axial wakefield in a GWFA is,

$$E_{zn}^{I}(x,z-ct) = \int_0^L \sum_{m=0}^{\infty} -4\pi\rho_0 x_0 \frac{d}{l}\left(\frac{\sin^2(pd/2)}{(pd/2)^2}\right)\left[\frac{\sin(ph)}{D(a,d,h,p)}\right]\cos\left[p_m(s-y')\right]\left(\frac{y'}{L}\right)\Theta(L-y')\,dy' \tag{16}$$

where $s = z - ct$, Assuming the $p_m \gg 1$

$$E_{zn}^{I}(x,z-ct) = \sum_{m=0}^{\infty} 4\pi\rho_0 x_0 \frac{d}{l}\left(\frac{\sin^2(pd/2)}{(pd/2)^2}\right)\frac{\sin(ph)}{D(a,d,h,p)\,p}\cos(p_m s+\delta_m) \tag{17}$$

where $\delta_m = \frac{\pi}{2} - p_m L$, $\pi\rho_0 x_0 c = I$ for current per unit length, Eq. (17) can be written as,

$$\frac{E_{zn}^{I}c}{4I} = \sum_{n=0}^{\infty}\frac{d}{l}\left(\frac{\sin^2(pd/2)}{(pd/2)^2}\right)\left[\frac{\sin(ph)}{p\left[hpa\frac{d}{l}\left(\frac{\sin^2(pd/2)}{(pd/2)^2}\right)\cos(ph)+\left\{a\frac{d}{l}\left(\frac{\sin^2(pd/2)}{(pd/2)^2}\right)+h\right\}\sin(ph)\right]}\right] \cos(p_m s+\delta_m) \tag{18}$$

Denoting $\bar{p} = pl$, $\bar{h} = (h/l)$, $\bar{d} = (d/l)$ and $\bar{a} = (a/l)$ as normalizing quantities,

$$\frac{E_{zn}^{I}c}{4I} = \sum_{n=0}^{\infty}\bar{d}\left(\frac{\sin^2(\bar{p}\bar{d}/2)}{(\bar{p}\bar{d}/2)^2}\right)\left[\frac{\sin(\bar{p}\bar{h})}{\bar{p}\left[\bar{h}\bar{p}\bar{a}\bar{d}\left(\frac{\sin^2(\bar{p}\bar{d}/2)}{(\bar{p}\bar{d}/2)^2}\right)\cos(\bar{p}\bar{h})+\left\{\bar{a}\bar{d}\left(\frac{\sin^2(\bar{p}\bar{d}/2)}{(\bar{p}\bar{d}/2)^2}\right)+\bar{h}\right\}\sin(\bar{p}\bar{h})\right]}\right] \cos(p_m s+\delta_m) \tag{19}$$

## 3. RESULT AND DISCUSSION

A theoretical work has been presented to analyze and calculate the wakefield amplitude and frequency in a grating wakefield accelerator. The analysis involves calculation in a dual planar grating facing each other and parallel to the axial electron beam. Fig. 2 displays the dispersion curve of the $TM_{01}$ mode of the dual-grating waveguide for fixed beam-grating gap and grating width. The curves are plotted for varying slot heights. The dispersion relation is plotted of the $TM_{01}$ mode of the grating guide for

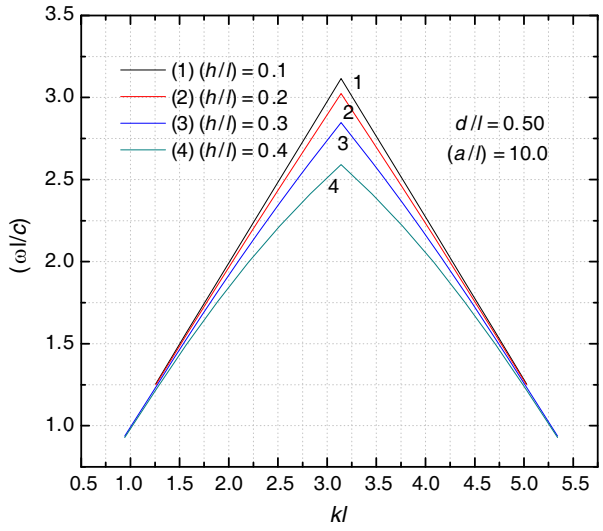


**Figure 2.** Dispersion curve of the $TM_{01}$ mode of grating waveguide.

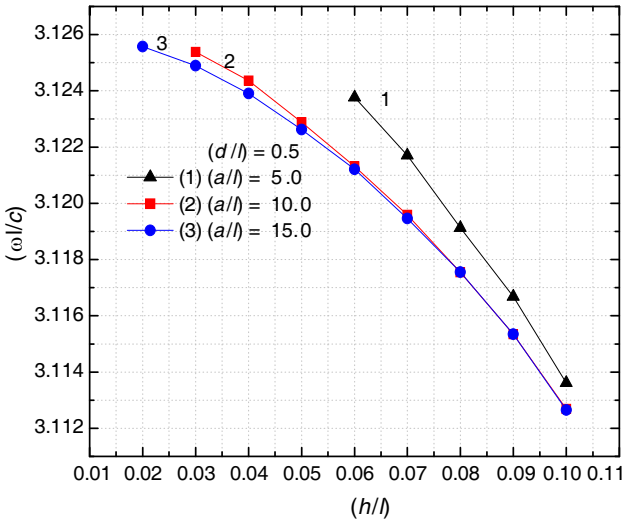


**Figure 3.** Normalized frequency versus grating slot heights.

$n = 0$ space harmonic $(0 < kl < \pi)$ and $n = -1$, $(\pi < kl < 2\pi)$ radiation field space harmonic. The dispersion curves move upward and approach the light line for shallower slot heights. Fig. 3 gives the normalized wakefield frequency, i.e., $\omega l/c$ for the lowest $TM_{01}$ mode as a function of the normalized slot heights. The grating period is the normalizing parameter. It has been seen for three values of $a/l$, i.e., $a/l = 5.0,\ 10.0,\ 15.0$, where $a$ is the distance of the grating surface from the waveguide axis. As the slot height increases, the wakefield frequency decreases. For a fixed slot height, the wakefield frequency decreases for increased beam-grating gap. Eq. (19) is the derived analytical formula for the normalized wakefield amplitude. It can be further analytically discussed under the assumption that the grating period is much less than the wave length, i.e., $l \ll \lambda$. Under this approximation, we substitute $\sin\theta \approx \theta$ and $\cos\theta \approx 1$ and rewrite Eq. (18) as, for $\bar{E}_{zg} = (E_z c/4I)$

$$\bar{E}_{zg} = \frac{1}{\dfrac{\omega l}{c}\left(\dfrac{2a}{l} + \dfrac{h}{d}\dfrac{(k_n d/2)^2}{\sin^2(k_n d/2)}\right)} \tag{20}$$

Equation (20) gives a transparent understanding of the wakefield accelerator in grating waveguide in terms of grating parameters. The wakefield amplitude decreases for deeper slot heights and increases for shallower slots for a fixed beam grating separation. For fixed slot heights, the decrease of the beam grating separation results with increased wakefield amplitude. The grating wakefield amplitude is inversely proportional to the wakefield frequency. In Fig. 4, we plot the normalized wakefield amplitude versus grating slot heights. It is observed that for closed beam grating gap, the wakefield amplitude falls rapidly with variation of the slot heights in comparison with larger beam grating separation. In Fig. 5, the wakefield frequency is plotted for typical parameters of slot width, slot heights, beam grating separation for grating period 100–200 μm range, and slot heights in 10–20 μm range. The grating waveguide is a useful THz wakefield accelerator. The dielectric liner wakefield accelerator is analyzed in detail by Sharma et al. [26] in a dual slab structure and by Garate and Fisher [27] in a cylindrical structure waveguide. It is shown that thin dielectric liners result in substantially lower wakefields than thicker liners and are not preferable in a dielectric wakefield accelerator. To compare the present results with previous results by Sharma et al. [26],

$$\bar{E}_{zd} = \frac{\sqrt{\varepsilon - 1}\sin(u(b-a))}{\sqrt{\varepsilon - 1}p\left\{ua(b-a)\cos(u(b-a)) + a\sin(u(b-a)) + \varepsilon(b-a)\sin(u(b-a))\right\}} \tag{21}$$

where, $\bar{E}_{zg} = (E_z c/4I)$, when $u = p\sqrt{\varepsilon - 1}$, $(b-a)$ is the dielectric thickness, and $b$ and $a$ are the outer and inner half width of the dielectric liner. $(a - x_0)$ is the beam-dielectric gap and $2x_0$ the beam

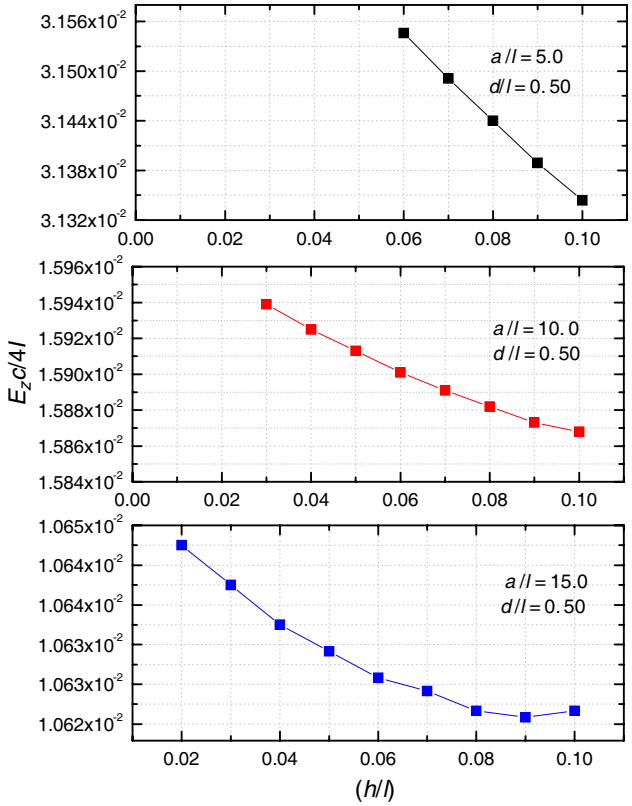


**Figure 4.** Normalized wakefield amplitude versus grating slot heights.

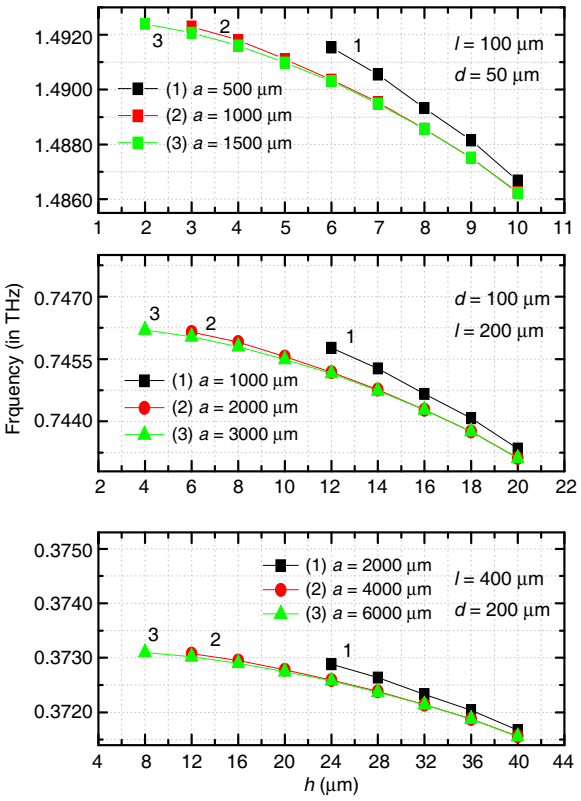


**Figure 5.** Frequency versus slot height.

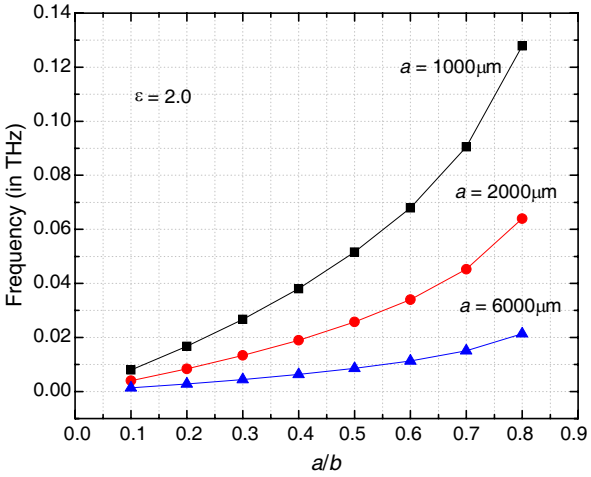


**Figure 6.** Frequency (in THz) versus $a/b$.

height. Under the approximation that the dielectric liner thickness is smaller than the wavelength, i.e., $(b-a) \ll \lambda$, Eq. (21) is written as,

$$\bar{E}_{zd} = \frac{1}{\left(\dfrac{\omega\,(b-a)}{c}\right)\left\{\dfrac{2a}{(b-a)} + \varepsilon\right\}} \tag{22}$$

Eq. (22) of the dielectric wakefield amplitude is analogous to Eq. (20) in terms of liner parameters. The variation of the dielectric wakefield frequency versus dielectric liner ratio is shown in Fig. 6 for $\varepsilon = 2$

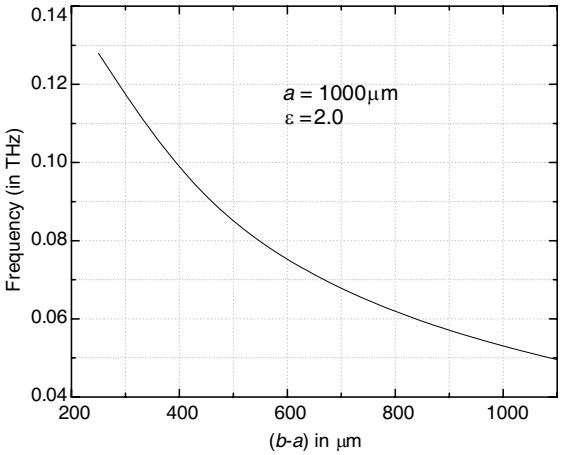


**Figure 7.** Frequency (in THz) versus dielectric liner thickness.

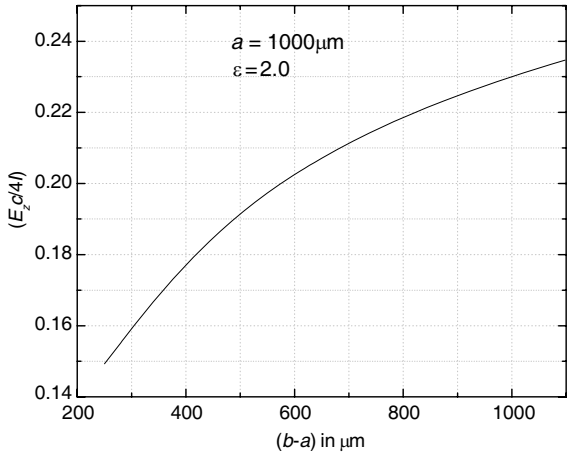


**Figure 8.** Normalized wakefield amplitude versus dielectric liner thickness.

and $a = 1\,\text{mm}$. For closer gap between beam and inner dielectric liner, the wakefield frequency is highly sensitive and shows a steep enhancement at thinner liner. As the liner thickness increases, the wakefield frequency moves away from the THz range. In Fig. 7, we plot the wakefield frequency versus dielectric liner thickness for $\varepsilon = 2$ and $a = 1\,\text{mm}$. The variation in wakefield amplitude with liner thickness is shown in Fig. 8. The expressions in Eq. (20) and Eq. (22) allow us to write,

$$\frac{\bar{E}_{zg}}{\bar{E}_{zd}} = \frac{f_d\left\{2a + \varepsilon\left(b - a\right)\right\}}{f_g\left\{2a + (hl/d)\right\}} \tag{23}$$

$f_d$ and $f_g$ are the dielectric and grating wakefield frequency, respectively. For material consideration, i.e., $\varepsilon > 1$, the dielectric wakefield accelerator operates below THz, and for $f_g > f_d$, we have $\bar{E}_{zg} < \bar{E}_{zd}$. For physical parameters considered here, we have $\frac{c}{4}E_{zd} = 0.23I$ and $\frac{c}{4}E_{zg} = 0.03I$. One needs higher beam currents in a grating structure than a dielectric liner structure to drive the same accelerating gradient wakefield at THz.

## 4. CONCLUSION

In this paper, we analyze the wakefield acceleration in a grating waveguide slow wave structure. It is shown that the accelerator is easily tuned at THz frequency. The results are compared with a dielectric wakefield accelerator. Dielectric wakefield accelerator gives larger axial wakefield for a lower dielectric constant liner for a given geometry. However, thinner liners are not preferable in dielectric wakefield accelerator, as they drive much lower wakefield [27] for a given current. This limits the application of dielectric wakefield accelerator towards THz range. Therefore, it is shown that the application of grating wakefield device as a practical accelerator is possible at THz without the disadvantages of a dielectric breakdown associated with a dielectric wakefield accelerator. The grating wakefield accelerator shares important analogies with both the dielectric wakefield accelerator and plasma wakefield accelerator. Just like the dielectric wakefield accelerator, it is an electromagnetic device driven by the waveguide mode. The plasma wakefield accelerator is a electrostatic accelerator driven by electron plasma wave. The grating wakefield accelerator shares an analogy with plasma wakefield accelerator in the sense that grating wakefield accelerator is too a single mode device expected to be as efficient as the plasma wakefield accelerator. In a dielectric wakefield accelerator, the drive beam propagates in vacuum very close to the vacuum-dielectric interface. A sufficient high wakefield amplitude results in creating a plasma due to dielectric ionization that short out the wakefield. This imposes an upper limit on the maximum accelerating gradient [28]. The accelerating gradient of the dielectric wakefield accelerator must be below the breakdown field of the dielectric material. The grating wakefield accelerator being a metallic grating surface does not suffer from dielectric breakdown.

## ACKNOWLEDGMENT

We are grateful to Prof. Y. C. Huang, National Tsing Hua University for many technical discussions on the topic of slow wave periodic structure waveguide for laser and accelerator applications. This work is supported by DRDO, New Delhi, India.

## REFERENCES

1. Keinigs, R., W. Peter, and M. Jones, "A comparison of the dielectric and plasma wakefield accelerators," *Physics Fluids B*, Vol. 1, No. 9, 1872, 1989.
2. Chen, P., J. M. Dawson, R. W. Huff, and T. Katosouleas, "Acceleration of electrons by the interaction of a bunched electron beam with a plasma," *Physics Review Letters*, Vol. 54, 693, 1985.
3. Ruth, R. D., A. Chao, P. L. Morton, and P. B. Wilson, *A Plasma Wake Field Accelerator*, 3374, SLAC-PUB, 1984.
4. Sotnikov, G. V., K. V. Galaydych, V. A. Kiselev, P. I. Markov, and I. N. Onishchenko, "Optimization of rectangular dielectric structures for the planned wake-field acceleration experiments in KIPT," *Proceedings of IPAC 2013*, TUPEA057, 1262, Shanghai, China, 2013.
5. Sotnikov, G. V., T. C. Marshall, and J. L. Hirshfield, "Co-axial two-channel high-gradient dielectric wake field accelerator," *Physical Review Special Topics-accelerators and Beams*, Vol. 12, 061302, 2009.
6. Plettner, T. and R. L. Byer, "Proposed dielectric-based microstructure laser-driven undulator," *Physical Review Special Topics — Accelerators and Beams*, Vol. 11, 030704, 2008.
7. Wang, C. and J. L. Hirshfield, "Theory for wake fields in a multi-zone dielectric lined wave guide," *Physical Review Special Topics — Accelerators and Beams*, Vol. 9, 031301, 2006.
8. Rosing, M. and W. Gai, "Longitudinal- and transverse-wake-field effects in dielectric structures," *Physical Review D*, Vol. 42, No. 5, 1829, 1990.
9. Keinigs, R. and M. E. Jones, "The Cherenkov wakefield accelerator," *Particle Accelerators*, Vol. 24, 223–229, 1989.
10. Garate, E., "Transverse wake fields due to nonaxisymmetric drive beams in the dielectric wake-field accelerator," *Physics Fluids B*, Vol. 3, No. 4, 1104, 1991.
11. Jing, C., A. Kanareykin, J. G. Power, M. Conde, W. Liu, S. Antipov, P. Schoessow, and W. Gai, "Experimental demonstration of wakefield acceleration in a tunable dielectric loaded accelerating structure," *Physical Review Letters*, Vol. 106, 164802, 2011.
12. Altmark, A. M., A. D. Kanareykin, and I. L. Sheinman, "Tunable wakefield dielectric-filled accelerating structure," *Technical Physics*, Vol. 50, No. 1, 87–95, 2005.
13. Kanareykin, A., et al., "Ferroelectric based technologies for accelerator component applications," *PAC 2007*, MOPAS087, Albuquerque, 2007.
14. Smith, S. J. and E. M. Purcell, "Visible light from localized surface charges moving across a grating," *Physics Review*, Vol. 92, No. 4, 1069, 1953.
15. Garate, E., R. Cherry, A. Fisher, and P. Philips, "High gain metal grating free electron laser," *Journal of Applied Physics*, Vol. 64, No. 12, 6618, 1988.
16. Andrews, H. L., J. E. Walsh, and J. H. Brownell, "Designing a grating based free electron laser," *Nuclear Instrument and Methods in Physics Research A*, Vol. 483, 478–481, 2002.
17. Maragos, A. A., Z. C. Ioannidis, and I. G. Tigelis, "Dispersion characteristics of a rectangular waveguide grating," *IEEE Transactions on Plasma Science*, Vol. 31, No. 5, 1075, 2003.
18. Walsh, J. E., "Electron beams diffraction gratings and radiation," *Nuclear Instrument and Methods in Physics Research A*, Vol. 445, 214–221, 2000.
19. Andrews, H. L., C. H. Boulware, C. A. Brau, J. T. Donohue, J. Gardelle, and J. D. Jarvis, " Effect of reflections and losses in Smith-Purcell free-electron lasers," *New Journal of Physics*, Vol. 8, No. 289, 16, 2006.

20. Andrews, H. L., C. A. Brau, and J. D. Jarvis, "Three-dimensional theory for a Smith-Purcell free-electron laser with grating sidewalls," *Proceedings of FEL'08*, MOPPH005, 17, Korea, 2008.
21. Li, D. and K. Imasaki, "Improvement of grating for smith-purcell device," *Terahertz Science and Technology*, Vol. 1, No. 4, 221, 2008.
22. Lu, Z.-G., Y.-B. Gong, Y.-Y. Wei, and W.-X. Wang, "Study of the double rectangular waveguide grating slow-wave structure," *Chinese Physics*, Vol. 15, No. 11, 2661, 2006.
23. Liu, W., Z. Liang, Z. Yang, D. Li, and K. Imasaki, "Two-stream Smith-Purcell free-electron laser using a dual-grating: Linear analysis," *Proceedings of FEL'06*, 111–114, Bessy, Berlin, Germany, 2006.
24. Li, D., Z. Yang, Y. Tsunawaki, M. R. Asakawa, M. Hangyo, et al., "Improve growth rate of Smith-Purcell free-electron laser by Bragg reflector," *Applied Physics Letters*, Vol. 98, 211503, 2011.
25. Prokop, C., P. Piot, M. C. Lin, and P. Stoltz, "Numerical modeling of a table-top tunable Smith-Purcell terahertz free-electron laser operating in the super-radiant regime," *Applied Physics Letters*, Vol. 96, 151502, 2010.
26. Sharma, G., G. Mishra, and Y. C. Huang, "Wakefield accelerator in a dielectric-plasma liner structure," *Nuclear Instrument and Methods in Physics Research A*, Vol. 648, 22, 2011.
27. Garate, E. and A. Fisher, "Transverse dimension effects in the dielectric wake-field accelerator," *Phys. Fluids B*, Vol. 2, No. 1, 179, 1990.
28. Sprangle, P., B. Hafizi, and R. F. Hubbard, "Ionization and pulse lethargy effects in inverse Cerenkov accelerators," *Physical Review E*, Vol. 55, No. 5, 5964, 1997.